ACS APPLIED MATERIALS & INTERFACES

Research Article

www.acsami.org

Induction of Osteogenic Differentiation of Human Adipose-Derived Stem Cells by a Novel Self-Supporting Graphene Hydrogel Film and the Possible Underlying Mechanism

Cheng-Qi Lyu,[†,¶] Jia-Yu Lu,[†,¶] Chun-Hua Cao,[†] Deng Luo,[‡] Yin-Xin Fu,[§] Yu-Shi He,[*,⊥] and De-Rong Zou[*,†]

[†]Department of Stomatology, Shanghai Jiao Tong University Affiliated Sixth People's Hospital, 600 Yishan Road, Shanghai 200233, China

[‡]Department of Endocrinology and Metabolism, Shanghai Key Laboratory of Diabetes Mellitus; Diabetes Institute, Shanghai Jiao Tong University Affiliated Sixth People's Hospital, 600 Yishan Road, Shanghai 200233, China

[§]Department of Clinical Laboratory, Pu'ai Hospital Affiliated to Tongji Medical College, Huazhong University of Science and Technology, Wuhan 430034, China.

[⊥]Shanghai Electrochemical Energy Devices Research Center, School of Chemistry and Chemical Engineering, Shanghai Jiao Tong University, Shanghai 200240, China

ABSTRACT: Graphene and its derivatives have received increasing attention from scientists in the field of biomedical sciences because of their unique physical properties, which are responsible for their interesting biological functions. With a range of extraordinary properties such as high surface area, high mechanical strength, and ease of functionalization, graphene is considered highly promising for application in bone tissue engineering. Here, we examined the effect of using a self-supporting graphene hydrogel (SGH) film to induce the osteogenic differentiation of human adipose-derived stem cells (hADSCs). In comparison to conventional graphene and carbon fiber films, the SGH film had higher mechanical strength and flexibility. Moreover, we found that the SGH film was nontoxic and biocompatible. Of particular interest is the fact that the film alone could stimulate the osteogenic differentiation of hADSCs, independent of additional chemical inducers. Such effects are stronger for the SGH film than for graphene or carbon fiber films, although the induction capacity of the SGH film is not as high as that of the osteogenic-induced medium. The excellent osteoinductivity of the SGH film is closely related to its remarkable physical properties that include specific nanostructures, surface morphology, strong cell adherence, reasonable surface hydrophilicity, and high protein absorption.

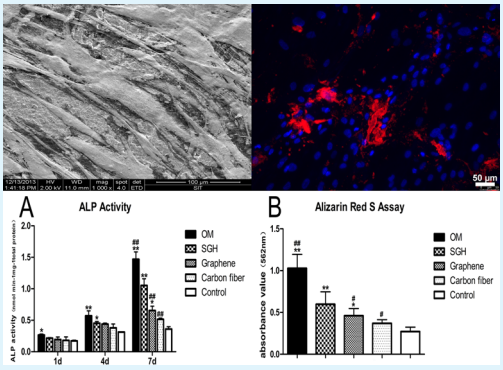

KEYWORDS: *graphene, hydrogel, human stem cells, cell differentiation, osteogenesis*

1. INTRODUCTION

Graphene has received increasing attention, especially in the fields of materials science, physics, chemistry, and nanotechnology, due to its unique physical properties including high electrical conductivity, elasticity, and high molecule absorption.[1] Although studies on graphene materials are still at a nascent stage, graphene has been widely used to help promote the development of stem cell and tissue engineering research.[2] For example, scientists found that induced pluripotent stem cells (iPSCs) cultured on graphene surfaces could spontaneously differentiate into ectodermal and mesodermal lineages.[3] Others observed that a graphene substrate could enhance the differentiation of human neural stem cells into neurons more effectively than a glass substrate after 30 days of culture.[4] In addition, graphene was found to enhance the cardiomyogenic differentiation of human embryonic stem cells (ESCs) when the graphene was coated with vitronectin (VN).[5]

However, despite its novel physical and biological properties that render it attractive for bioengineering, graphene is not yet ready for widespread biomedical application. The use of graphene is hampered by fears regarding the potential health risks of chemically modified materials.[6−8] The effects of graphene on human health might manifest at the cellular, tissue, and whole body levels. At the cellular level, the material could interact with biomolecules, disrupt cellular processes, and lead to cellular damage. At the tissue level, carbon nanomaterials could accumulate in tissues with long-term exposure and become difficult to eliminate. Undoubtedly, the continuous

Received: June 29, 2015
Accepted: August 26, 2015
Published: August 26, 2015

DOI: 10.1021/acsami.5b05802
ACS Appl. Mater. Interfaces 2015, 7, 20245−20254

Table 1. Sequence of Primers Used for RT-PCR

gene	forward primer sequence (5−3)	reverse primer sequence (5−3)
GAPDH	TTCGACAGTCAGCCGCATCTT	ATCCGTTGACTCCGACCTTCA
ALP	TCAAACCGAGATACAAGCAC	CCACCAGCAAGAAGAAGC
BMP2	GAGAAGGAGGAGGCAAAGAAA	AGCAGCAACGCTAGAAGACAG
RUNX2	AGTGGACGAGGCAAGAGTTTC	CCTTCTGGGTTCCCGAGGT
OCN	AGGGCAGCGAGGTAGTGAA	TCCTGAAAGCCGATGTGGT

accumulation of nanomaterials could pose a risk to organ function and therefore to health. Previously, we designed a novel, flexible, chemically modified, and self-sustained graphene hydrogel (SGH) film by rationally manipulating the colloidal interactions among solvated graphene sheets.[9] As described in our previous report, such a film is composed purely of graphene and has a simple multilayered structure.

Recently, a series of studies have shown that graphene promotes the *in vitro* proliferation and osteogenic differentiation of stem cells.[10−12] Therefore, we evaluated the applicability of the SGH film as a novel biocompatible material for bone regeneration. In our previous study, both the biocompatibility of the SGH film and the host tissue response were investigated *in vivo* after implantation into the subcutaneous tissue of rats. We found that the SGH film exhibited biocompatibility and extremely limited toxicity. Moreover, we also observed that the SGH film alone could stimulate osteogenic differentiation of rat bone marrow stromal stem cells, independent of additional inducers, both *in vitro* and *in vivo*. The biocompatibility and osteoinductive capacity of the SGH film suggests that it has potential for use in bone regenerative medicine.

Although scientifically promising, the mechanism through which graphene exerts its biological activity is not fully understood. In addition, we wondered whether the new modified graphene-based material is suitable for inducing the osteogenic differentiation of human adipose-derived stem cells (hADSCs). Therefore, the aim of this study was to test the *in vitro* effects of the SGH film on the osteogenic differentiation of hADSCs and to understand the underlying mechanism. We compared the mechanical and biological properties of the SGH film to those of other biomaterials including graphene and carbon fiber. Our results will help increase knowledge regarding SGH films and provide valuable information for future efforts to exploit graphene for human bone healing and regeneration.

2. MATERIALS AND METHODS

2.1. Preparation and Characterization of Self-Assembled Biomaterial Films. SGH and graphene films used in our experiments were manufactured by vacuum filtration of graphene dispersions, as described previously.[13,14] Briefly, a certain amount of chemically converted graphene (CCG) dispersion[15] was filtered through a mixed cellulose ester filter membrane via direct-flow vacuum filtration. The thickness and homogeneity of the films were strictly controlled since the physical properties of manufactured carbon graphene are strongly influenced by the number of graphene layers. Carbon fiber films were purchased from Fuel Cell Company (AvCarb P75, Fuel Cell Store, USA) for this experiment.

To evaluate the biocompatibility and bioactivity of the films, unseeded films and films seeded with ADSCs were rinsed in 0.1 M phosphate buffer (pH 7.2) and fixed with 2.5% glutaraldehyde in 0.1 M phosphate buffer for 2 h at 4 °C. The samples were dehydrated with ethanol and then placed in pure tert-butanol for 30 min. The cell-seeded films were gold-coated and analyzed using a scanning electron microscope (FEI Quanta 200 FEG, FEI, USA). In addition, the contact angle between the film surface and a water droplet was measured to further evaluate the surface hydrophilicity of the carbon fiber, graphene, and graphene−hydrogel membranes.[16−18] The contact angles were measured using a contact angle instrument (DSA30 KRÜSS, GmbH, Germany).

A bovine albumin serum (BSA) adsorption experiment[19,20] was conducted to investigate the adsorption characteristics of three films using the BCA Protein Assay Kit (Pierce Biotechnology, Inc., USA). First, these three films were modified to 1 cm in diameter and plated on 24-well plates. A BSA solution was prepared at a concentration of 250 μg/mL (pH 7.0) and was added to each well (500 μL/well) and incubated at 37 °C. After 1, 2, 8, and 12 h following BSA addition, the absorbance of the solution was measured at 450 nm using a microplate reader (iMark, Bio-Rad, USA).

2.2. Isolation, Culture, and Identification of ADSCs. Human ADSCs were isolated from liposuction aspirates harvested at the Sixth People's Hospital of Shanghai Jiao Tong University (Shanghai, China) following the ethical guidelines of the University. All patients (age range: 20−30 years old) provided informed consent for harvesting their adipose tissue. Donors with infectious or systemic diseases or malignancies were excluded from this study. The tissue was cultured as described previously.[21−23] After collagenase digestion and differential centrifugation, the isolated cells were monolayer-cultured in a low-glucose Dulbecco's modified Eagle medium (DMEM) containing 10% fetal bovine serum (FBS) and 1% penicillin/streptomycin at 37 °C with humidified air containing 5% CO_2. After 7 days of primary culture, cells were passaged and expanded for future use. The cells used in the present study were from passages 3−5.

For hADSC characterization, cell surface markers were quantified by flow cytometry as previously described.[24] ADSCs of passage 3 were harvested by treatment with 0.25% trypsin-EDTA (Gibco,USA). Trypsinized cells (5×10^6 cells) were washed twice with phosphate buffered saline solution (PBS) and stained with phycoerythrin (PE)-conjugated mouse antihuman CD29, allophycocyanin (APC)-conjugated CD34, fluorescein isothiocyanate (FITC)-conjugated mouse antihuman CD44 and CD45 (BD Biosciences, San Jose, CA), and mouse antihuman CD105 (Abcam, ab114052). Cells were stained with FITC- or PE-labeled mouse IgG (BD Biosciences) as a negative control. After 30 min of incubation at room temperature, the cells were washed twice with PBS. The samples were washed and then analyzed by EasyCyte HT (Guava, USA) with GuavaSoft 2.5.

For characterization of multipotent differentiation, ADSCs were seeded at a density of 4000 cells/cm^2 and cultured in human adipose-derived stem cell basal medium with preselected fetal bovine serum and osteogenic supplements (HUXMD-90021, Cyagen Biosciences,USA). After 21 days of incubation with osteogenic medium (OM), the mineral deposition in the extracellular matrix was visualized by staining with alizarin red S (A5533, Sigma,USA). For adipogenic induction, ADSCs were seeded at a density of 4000 cells/cm^2 and cultured in serum containing adipogenic medium (HUXMD-90031, Cyagen Biosciences). After 14 days of adipogenic induction, lipid droplets were observed by staining with Oil Red O (O0625−25G, Sigma).

2.3. Morphology and Vitality of ADSCs on Various Films. The ADSCs were cultured on different films including SGH, graphene, and carbon fibers for 1, 4, and 7 days in growth medium and then fixed in 2.5% glutaraldehyde overnight at 4 °C and freeze-dried (Alpha 1−2; Christ, Germany). Finally, the samples were sputter-coated with gold and examined by SEM to observe the adhesion and growth of ADSCs on the films. Additionally, staining for living and dead cells was used to evaluate cell attachment and viability of ADSCs seeded on three

DOI: 10.1021/acsami.5b05802
ACS Appl. Mater. Interfaces 2015, 7, 20245−20254

different biomaterial interfaces.[25,26] Briefly, seeded and control films were incubated for 45 min at room temperature with a mixture of 5 mM CellTracker green (5-chloromethylfluorescein diacetate; Molecular Probes, Eugene, OR) and 2.5 mM ethidium homodimer-1 (Molecular Probes). The viable cells (green fluorescence) and necrotic cells (red fluorescence) were examined using a fluorescence microscope and counted using the software Image-Pro Plus 6.0.

2.4. Quantitative Real-Time Polymerase Chain Reaction (qRT-PCR). The hADSCs were seeded onto SGH, graphene, or carbon fiber films in growth medium (DMEM supplemented with 10% fetal bovine serum). The hADSCs were seeded onto glass slides in either growth medium or osteogenic medium (growth medium with 50 μg/mL L-ascorbic acid, 10 mM glycerophosphate, and 100 nM dexamethasone). The expression of several osteogenic genes including Runx2 (runt-related transcription factor 2), ALP (alkaline phosphatase), BMP2 (bone morphogenetic protein 2), and OCN (osteocalcin) from ADSCs at passage 3 at 1, 7, and 15 days was analyzed by RT-PCR (Table 1). Briefly, RNA extraction was performed using PrimeScript RT Reagent Kit (RR047A, Takara, Japan) according to the manufacturer's instructions. The RNA was treated with DNase for 20 min to remove genomic DNA contamination from the samples. The cDNA was synthesized using oligo-dT primers from the total mRNA, and 200 ng of the cDNA was used for RT-PCR analysis (7900 HT, Applied Biosystems, Inc., USA). TaqMan Universal PCR mix, gene-specific primers (Sangon Biotech Inc., China), and cDNA were combined according to the manufacturer's instructions. The PCR reaction was performed as follows: 50 °C for 2 min, 95 °C for 10 min; 40 cycles of 95 °C for 15 s and 60 °C for 1 min. GAPDH was used as an endogenous control. The average cycle threshold (C_t) of three to six replicates was used for the calculation of the expression level (relative expression = $2 - (C_{t,\ sample} - C_{t,\ GAPDH})$. Three to six samples from each group were used for gene analysis. Each experiment was performed in triplicate. The primers for the target genes are listed in Table 1.

2.5. Assessment of Cellular Alkaline Phosphatase (ALP) Activity. The hADSCs were seeded onto three different films or onto glass slides in either growth medium or osteogenic medium. At 1, 4, and 7 days after cell seeding, ALP activity was evaluated as previously described.[27−29] Unseeded ADSCs (no films present) were used as a negative control. Briefly, the cells were detached from discs using trypsin-EDTA and resuspended in lysis buffer with 0.2% NP-40. Each sample was mixed with 1 mg/mL p-nitrophenyl phosphate (pNPP, Sigma, USA) in 1 M diethanolamine buffer as the substrate and incubated at 37 °C for 15 min. The reaction was stopped by the addition of 3 N NaOH. ALP activity was quantified by absorbance at 405 nm (ELX808; Biotek, USA). Total protein content was determined with the Bradford method using the Bio-Rad protein assay kit (Bio-Rad, USA) and a BSA standard (Sigma, USA). ALP activity was calculated as absorbance at 405 nm (OD value) per milligram of total cellular proteins. All experiments were performed in triplicate.

2.6. Immunofluorescence Staining for BMP2, OCN, and Runx2. The ADSCs were collected, fixed with 4% paraformaldehyde for 10 min, rinsed with PBS, and treated with 0.3% Triton X-100 for 10 min. After blocking with 5% bovine serum albumin at 37 °C for 1 h, the ADSCs were incubated with mouse anti-Runx2, mouse antiosteocalcin antibody, and mouse anti-BMP2 antibody at 37 °C for 1 h. Cells were further incubated with FITC-Affinipure goat antimouse IgG antibody (Jackson ImmunoResearch, USA) at 37 °C for 1 h. Cells were counterstained with DAPI at 10 μg/mL, at room temperature for 8 min, and washed with PBS three times. They were then mounted with antiquench reagent and observed under a fluorescent microscope (DMI6000 B, Leica, Germany).

2.7. Fluorescence and Semiquantitative Analysis for Mineralization. Primary ADSCs (passage 3) at 21 days cultured *in vitro* were used for this assay. First, the mineral deposition in the extracellular matrix was analyzed by staining with 10 mg/L alizarin red S for 5−7 days before observation and subsequent visualization using a fluorescent microscope (DMI6000 B, Leica, Germany).

Semiquantitative analysis was performed to further quantify the level of mineralization, particularly calcium-containing nodules, at 21 days.[30] Briefly, the cells were washed with PBS and fixed with 4% paraformaldehyde at 4 °C for 30 min. The cells were then rinsed in distilled water, stained with alizarin red S at pH 4.2 with rotation for 15 min at room temperature, and then washed extensively with water. Dye was eluted in 10% w/v hexadecylpyridinium chloride monohydrate (30037326, Sinopharm Chemical Reagent Co., Ltd., China) in 10 mM sodium phosphate (pH 7.0), and the concentration was determined by absorbance at 562 nm.

2.8. Statistical Processing. Data were expressed as the mean ± SD and analyzed with SPSS 18.0 software. The significance of differences was assessed by one-way analysis of variance (ANOVA). $p < 0.05$ was considered statistically significant.

3. RESULTS

3.1. Mechanical and Biological Properties of Tested Films. As shown in Figure 1, panels A−F, SGH and graphene

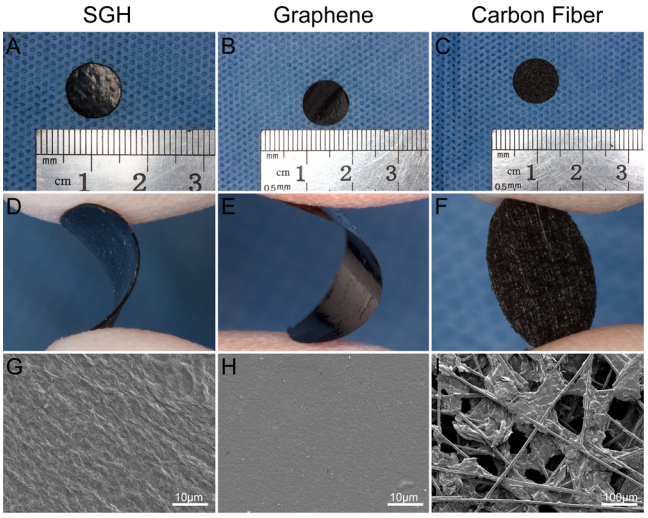

Figure 1. Structure and characterization of carbon fiber, graphene, and graphene-derived films. (A, B, and C) Photograph of three different films. (A) SGH; (B) graphene; (C) carbon fiber. (D, E, and F) Physical characteristics and properties, including flexibility, of three films. (D) SGH; (E) graphene; (F) carbon fiber. (G, H, and I) Microstructure of three films by SEM. Left, SGH; middle, graphene; right, carbon fiber. The scale bars for panels G and H are 10 μm. The scale bar for panel I is 100 μm.

films have higher mechanical strength and higher flexibility than conventional carbon fibers. Graphene film has a relatively a smooth surface, whereas carbon fiber film has a rough surface; SGH is smoother than carbon fiber but rougher than graphene. The microstructures of the three films were observed by SEM (Figure 1G−I). The SGH film had a nanoporous corrugated morphology, the self-supporting graphene surface was free of fine lines and large pores at the nanoscale, and the carbon fiber materials exhibited massive fibrous carbon structures without nanostructures.

BSA molecules adsorbed more effectively onto the SGH surface than the graphene or carbon fiber films after 2, 8, and 12 h of BSA treatment, although no significant differences were observed in the first hour of treatment (Figure 2A). After 12 h of treatment, the protein absorption rates were approximately 59.09 ± 10.30 μg on SGH, 22.33 ± 7.91 μg on the self-supporting graphene surface, and 26.19 ± 8.34 μg on the carbon fiber film. The protein absorption rate onto the SGH film was significantly higher than for the other carbonaceous

DOI: 10.1021/acsami.5b05802
ACS Appl. Mater. Interfaces 2015, 7, 20245−20254

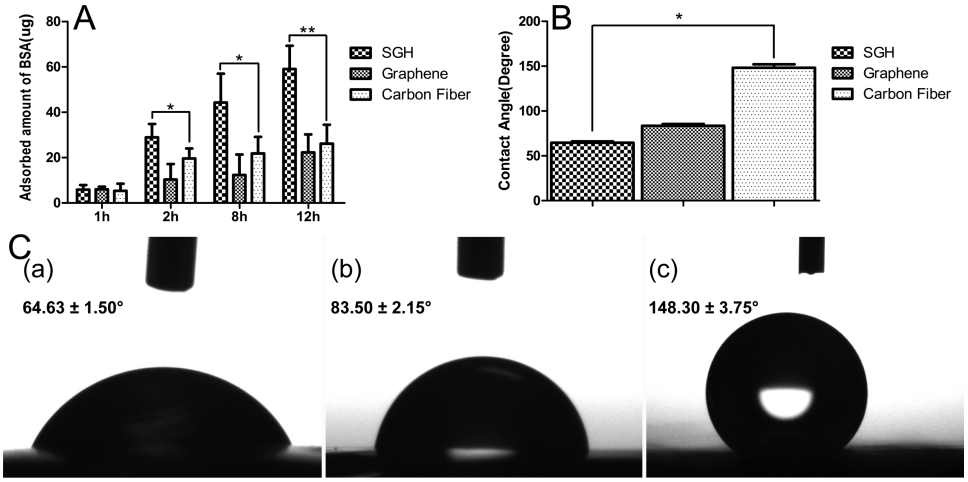

Figure 2. Biological properties of carbon fiber, graphene, and graphene-derived films. (A) Evaluation of protein adsorption on tested film surfaces. (B) Degree of hydrophilicity expressed as the contact angle between the surface and water droplet. (C) Hydrophilic surface of three films: (a) SGH; (b) graphene; (c) carbon fiber. *, $p < 0.05$; **, $p < 0.01$.

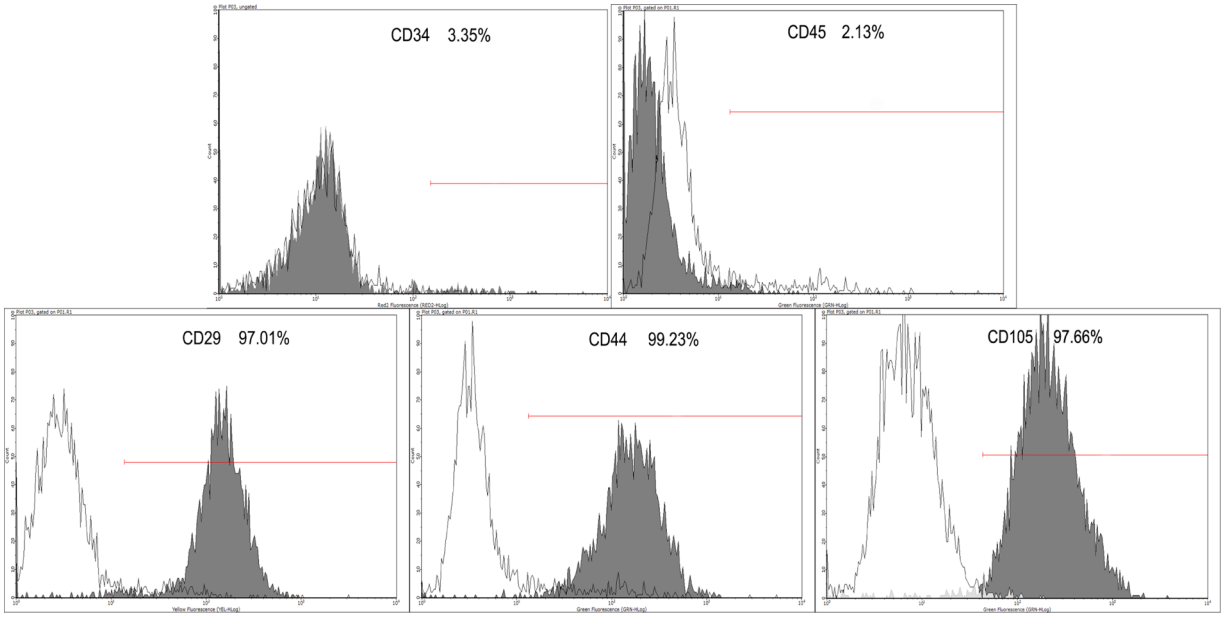

Figure 3. Characterization of hADSCs using flow cytometry. Most ADSCs expressed CD29, CD44, and CD105, whereas most were negative for CD34 and CD45. Horizontal lines on the graphs indicate the distribution range of positive-labeled cells for each marker.

films ($p < 0.05$). In addition, contact angles on the surfaces of these films were also determined in air and under water (Figure 2B,C). The contact angles were 64.63 ± 1.50°, 83.50 ± 2.15°, and 148.30 ± 3.75° in SGH, self-sustaining graphene, and carbon fiber films, respectively. The SGH film produced a smaller contact angle ($p < 0.05$), which indicates higher surface hydrophilicity than the other carbonaceous films. Together, our results indicate that ADSCs more effectively adapt, proliferate, and differentiate on SGH surfaces, probably because the SGH film has a high specific surface area, nanoscale morphological features, and high adsorption capacity.

3.2. Characterization of ADSCs and Multipotent Differentiation Potential *in Vitro*. Cell surface marker analysis by flow cytometry revealed that these fibroblast-like cells expressed high levels of the MSC markers CD29, CD44, and CD105, and rarely expressed both CD45 and CD34, which are hematopoietic stem cell markers (Figure 3). After expansion to passage 3 under normal growth conditions, ADSCs exhibited an elongated fibroblast-like morphology *in vitro* (Figure 4A,B).

ADSCs displayed an irregular polygonal morphology after 21 days of osteogenic induction. Mineralized nodular structures appeared after 21 days and were assessed by Alizarin Red S, which was localized to the calcium deposits (Figure 4C).

In addition, adipogenesis and lipid vacuole formation in ADSCs were confirmed by staining cells with the lipid dye Oil Red O.[31] Generally, ADSCs started exhibiting a round shape after 6−7 days in adipogenic medium. After 14 days of induction of adipogenic differentiation, lipid droplets continuously and increasingly accumulated in the cytoplasm of differentiated ADSCs; lipid-rich intracellular vacuoles were confirmed by Oil Red O staining (Figure 4D).

3.3. Morphology and Vitality of ADSCs on Various Films. To compare the biocompatibility of SGH films to that of other films, the morphology of ADSCs on various films after 1, 3, and 7 days of culture was observed by SEM (Figure 5). We

DOI: 10.1021/acsami.5b05802
ACS Appl. Mater. Interfaces 2015, 7, 20245−20254

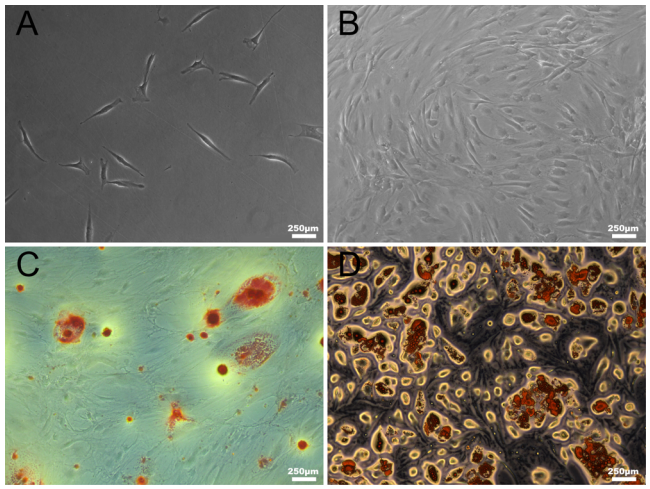

Figure 4. Multipotent differentiation potential of ADSCs *in vitro*. (A, B) ADSCs cultured at passages 0 and 3. (C) ADSCs were treated for 21 days with osteogenic medium (OM). Osteogenic differentiation was determined by alizarin red S staining of calcium deposits (mineralization). (D) After 14 days of adipogenic differentiation, the cells were fixed and stained with Oil Red O for lipid droplets. The scale bar is 250 μm.

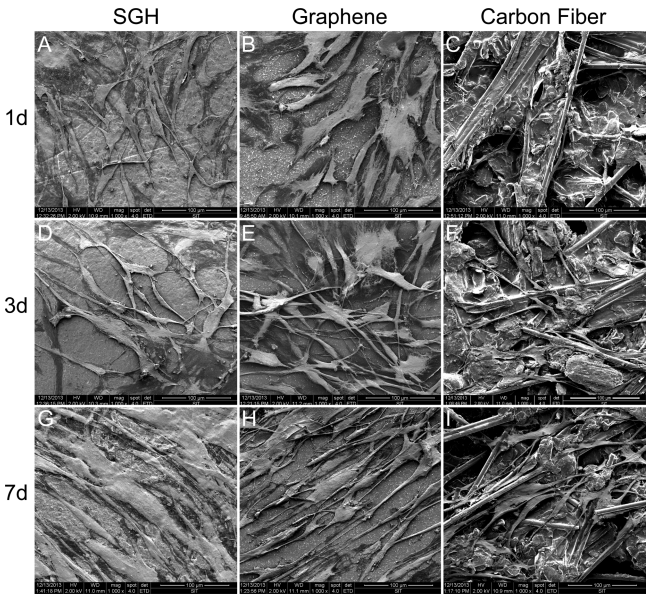

Figure 5. Cell attachment, proliferation, and morphological changes on SGH, graphene and carbon fiber films. (A) SGH film, (B) graphene film, and (C) carbon fiber film at day 1 after seeding. (D) SGH film, (E) graphene film, and (F) carbon fiber film at day 3 after seeding. (G) SGH film, (H) graphene film, and (I) carbon fiber film at day 7 after seeding. The scale bar is 100 μm.

observed that cells cultivated on SGH films were spread out and appeared confluent, indicating that cell attachment was stronger than that observed for the other two films. The ADSCs attached tightly to the surface of the SGH film and appeared flat in shape at day 1 after seeding, spread out by day 3, and reached a high cell density at day 7 (Figure 5A,D,G). Cells cultivated on graphene films also exhibited a flat, well-spread morphology similar to cells seeded on SGH films but remained at relatively low cell densities (Figure 5B,E,H). In contrast, cells were round in shape on carbon fiber films at day 1 after seeding and were distributed sporadically at very low densities after 7 days of culture (Figure 5C,F,I).

Cell viability of ADSCs on SGH film and other films was measured after 1 and 3 days of culture, and it was found that ADSCs maintained high viability on all scaffolds (Figure 6A). After 1 day of culture, cell viability, expressed as the ratio of live to dead cells, was 95.43 ± 0.96%, 94.94 ± 1.70%, and 89.97 ± 1.54% on self-sustaining graphene hydrogel, self-sustaining graphene, and carbon fiber film, respectively (Figure 6B). After 3 days of culture, the ratio of live to dead cells was 97.64 ± 0.95%, 95.40 ± 1.40%, and 94.80 ± 1.32%, respectively. There was a slight different between the SGH film and carbon fiber film in the initial day 1 of culture, but no difference was observed at day 3. This implies that the SGH film, similar to conventional graphene and carbon fiber, is nontoxic to normal cells. Taken together, ADSCs more strongly adhere, adapt, and proliferate on SGH surfaces, indicating that SGH films are more biocompatible than other films.

3.4. Effects of SGH Film on the Osteogenic Differentiation of ADSCs. *3.4.1. Gene Expression during Differentiation of ADSCs into Osteoblasts.* The expression of specific osteogenic mRNA was used to assess the differentiation of ADSCs into an osteoblastic lineage (Figure 7). The negative control for each experiment was ADSCs cultured on glass (control group), which expressed no detectable levels of any of the tested osteogenic specific genes. In addition, osteogenic differentiation was induced on glass with osteogenic medium, which served as a positive control, producing significantly higher osteogenic-specific gene expression. We first examined the expression of ALP, an early stage osteoblast differentiation marker. On day 1, the ALP expression level was much higher in the OM group (on glass) than on any films or surfaces without OM. In the absence of OM, on day 1, there were no differences in ALP expression for ADSCs seeded on SGH film, graphene film, carbon fiber film, or glass. The ADSCs on the SGH film, in the absence of OM, produced higher ALP expression levels than ADSCs on the graphene film, carbon fiber film, or glass at day 7 and 15. However, at day 7 and 15, the level of ALP expression for ADSCs on SGH film in the absence of OM was still lower than the ALP expression for cells on glass with OM.

BMP-2 is an early marker of osteogenic differentiation. We found that cells seeded on the SGH film expressed significantly higher levels of BMP2 than cells on graphene film, carbon fiber film, or glass at days 7 and 15. The same general trend was observed for Runx2 expression, which was generally lower for cells on self-sustaining graphene than for cells on SGH film ($p < 0.05$). Similar results were also observed for the expression of OCN, a late osteogenic marker.

3.4.2. Characterization of Differentiated ADSCs by Immunofluorescence Staining. ADSCs seeded onto various surfaces and films, including differentiated and undifferentiated cells, were subjected to immunocytochemistry using antibodies against osteogenic differentiation markers (Runx2, BMP2, and OCN). As shown in Figure 8, these markers were apparent in cells seeded onto SGH films, graphene, or glass with OM at day 15. However, nothing but DAPI staining was apparent for cells on carbon fiber or glass without OM. Moreover, we observed that cells on graphene were positive for BMP2 and Runx2, but negative for OCN. However, BMP2 and Runx2 were expressed at much higher levels in cells on the SGH film than in cells on glass with OM. Cells on the SGH film also showed markedly stronger staining for BMP2 and Runx2 than the graphene group. Moreover, cells on SGH film at 21 days had significantly

DOI: 10.1021/acsami.5b05802
ACS Appl. Mater. Interfaces 2015, 7, 20245−20254

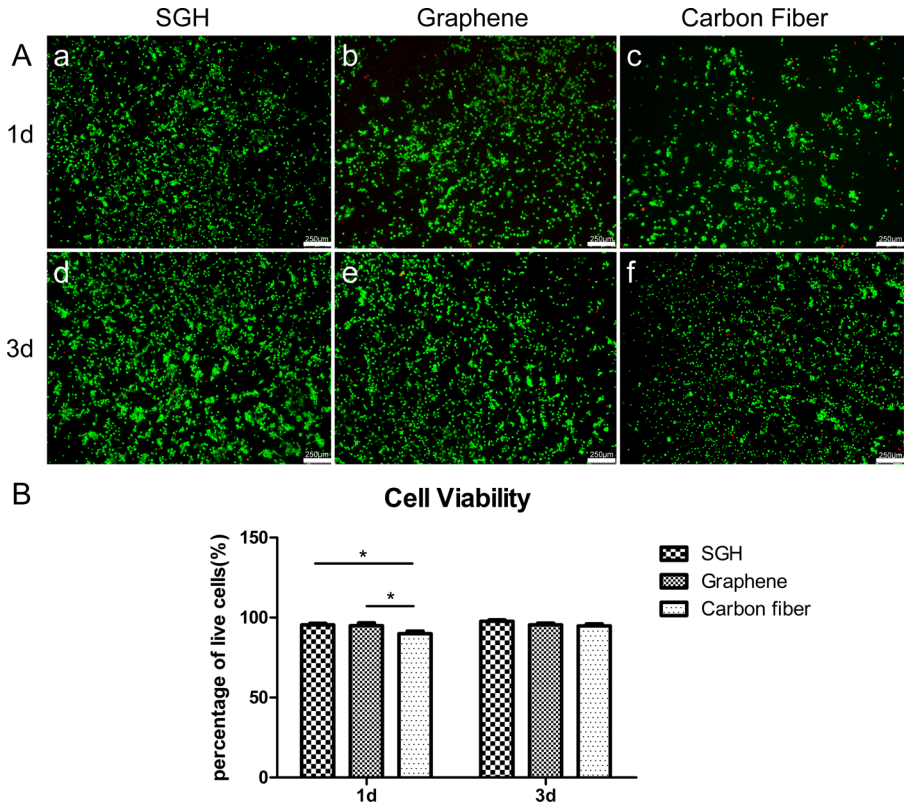

Figure 6. Measurements of ADSC viability on different films at day 1 and day 3 of culture. (A) Live/dead double staining of ADSCs (a and d, SGH; b and e, graphene; c and f, carbon fiber; live cells were stained florescent green, and dead cells appeared red). (B) Living and dead ADSCs on carbon fiber, graphene, and graphene-derived films. The scale bar is 250 μm. ∗, $p < 0.05$.

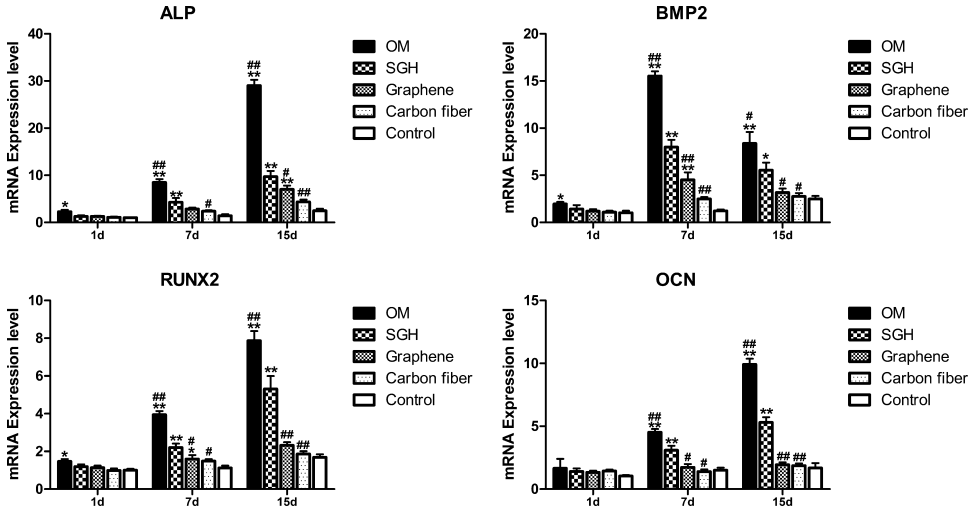

Figure 7. Quantitative RT-PCR analyses for the expression of genes mediating osteogenesis and differentiation processes. Results are the means ± SDs for triplicate measurements. Expression of the following genes was tested: ALP, alkaline phosphatase; BMP2, bone morphogenetic protein 2; RUNX2, runt-related transcription factor 2; OCN, osteocalcin. ∗, $p < 0.05$ and ∗∗, $p < 0.01$ versus the negative control group. #, $P < 0.05$ and ##, $P < 0.01$ versus the SGH group. SGH film, graphene, and carbon fiber groups were treated with growth medium. Negative control: ADSCs on glass with growth medium. Positive control: ADSCs on glass with osteogenic medium.

greater calcium levels than graphene, although the amount was lower than for cells on glass with OM. Our results suggest that SGH is a novel self-sustaining graphene film that has higher potential to induce the differentiation of ADSCs into osteoblasts than either graphene or carbon fiber films.

3.4.3. ALP and Alizarin Red S Calcium Nodule Staining. To evaluate the overall osteogenic differentiation of the hADSCs on the various films, endogenous alkaline phosphatase activity and cell-mediated calcium mineralization were evaluated. Figure 9, panel A shows the sequential development of alkaline phosphatase activity in each group over 7 days *in vitro*. Except for the OM group, there were no differences between the groups on the first day of culture. However, the SGH group displayed stronger ALP activity than the other groups at days 4 and 7, but still had lower activity than the OM group. In addition, mineralization was determined by semiquantitative

DOI: 10.1021/acsami.5b05802
ACS Appl. Mater. Interfaces 2015, 7, 20245−20254

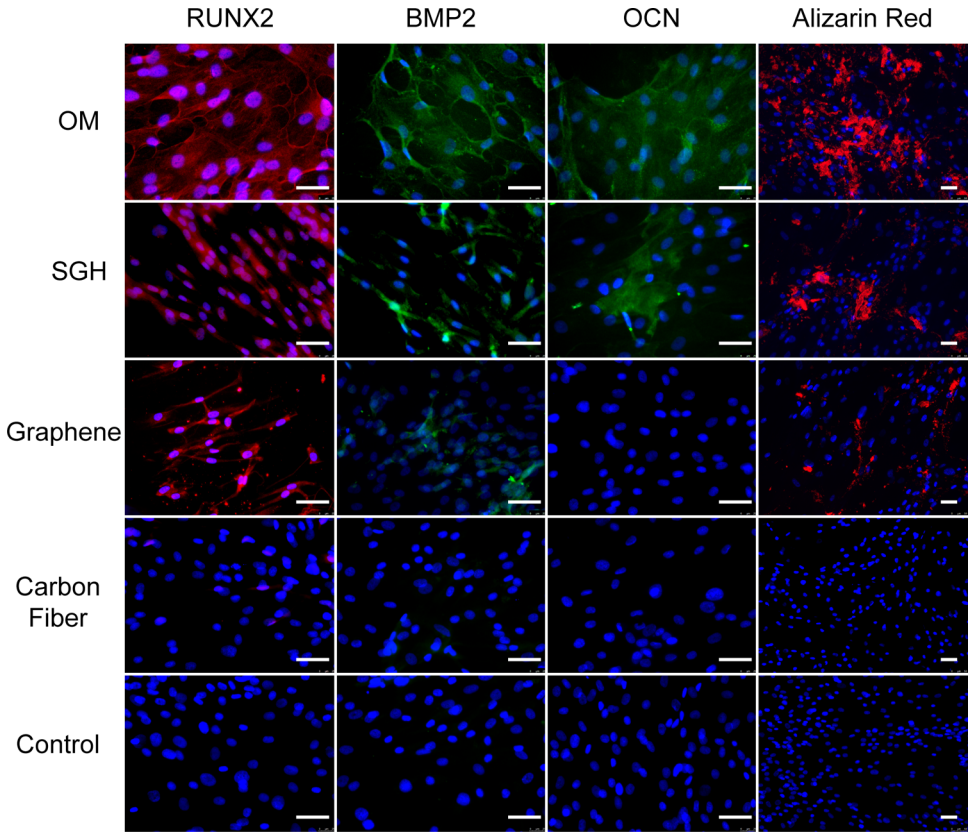

Figure 8. Immunofluorescence staining for BMP2, OCN, and RUNX2 in differentiated ADSCs at 15 days and alizarin red S (ARS) staining for mineralized nodules at 21 days. SGH film, graphene, and carbon fiber groups were treated with growth medium. Negative control: ADSCs on glass with growth medium. Positive control: ADSCs on glass with osteogenic medium. The scale bar is 50 μm.

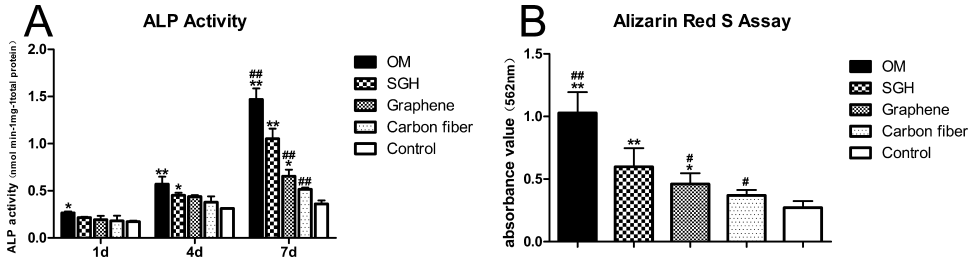

Figure 9. Assessment of cellular ALP activity and mineralization of ADSCs on films during *in vitro* osteogenic differentiation. (A) ALP activity of ADSCs at 1, 4, and 7 days. (B) Semiquantitative analysis of in vitro mineralization. SGH film, graphene, and carbon fiber groups were treated with growth medium. Negative control: ADSCs on glass with growth medium. Positive control: ADSCs on glass with osteogenic medium. *, $p < 0.05$ and **, $p < 0.01$ versus the negative control group. #, $p < 0.05$ and ##, $p < 0.01$ versus the SGH group.

analysis for each group at day 21. The total mineralized matrix volume increased with time for cells on SGH film, graphene film, and glass with OM, but not for cells on carbon fiber or glass without OM (Figure 9B).

4. DISCUSSION

In the present study, we found that the SGH film significantly supported more effective bone regeneration than traditional graphene and carbon fiber films due to a combination of properties including specific nanostructures, strong cell adherence, better protein absorption rates, and high surface hydrophilicity. The present study has deepened our understandings of the biological behavior of the SGH film.

In fact, stem cells harvested from fatty tissue have been shown to harbor significant potential for tissue repair in a wide variety of disease models including hypoxia-induced neuronal damage, liver failure, heart disease, and Parkinson's disease.[32] A recent report also demonstrated that human ADSCs have the ability to prevent cisplatin-induced kidney injury *in vivo* by decreasing renal tubular apoptosis, suppressing inflammation, and secreting the renal-protective factor HIF-1α.[33] Likewise, several groups have reported improved outcomes in animal models of diabetes following transplantation of genetically modified or chemically induced ADSCs.[34−36] The combination of stem cells and biomaterial scaffolds is currently a very promising strategy for restoring tissue functions.[37,38] Although major advances have been made in this field, many challenges remain.[39]

There are many possible factors influencing how scaffold materials elicit bone regeneration and repair including the surface characteristics of materials, forces generated at the cell/material interfaces, surface hydrophilicity, and the rate of

DOI: 10.1021/acsami.5b05802
ACS Appl. Mater. Interfaces 2015, 7, 20245−20254

protein adsorption.[40] Although graphene can induce osteogenesis, it can be chemically modified or combined with other materials like hydrogels, polymers, ceramics, and metals to further strengthen its osteoinductive potential. Graphene oxide nanoflakes incorporated into gelatin-hydroxyapatite scaffolds enhanced osteogenic differentiation of human mesenchymal stem cells in the absence of osteogenic inducers such as dexamethasone, L-ascorbic acid, or β-glycerophosphate.[41] Surface modification of multipass caliber-rolled titanium alloy with dexamethasone-loaded graphene significantly enhanced growth and differentiation of MC3T3-E1 cells into osteoblasts.[42] Other researchers have also reported similar results. Wall et al.[43] demonstrated that titanium modified to have rough surfaces and high hydrophilicity exhibited increased osteoinductive capacity. In our previous studies, we optimized the fabrication of graphene-based films.[9] A hydrogel was introduced to improve the strength and flexibility of graphene film. Our results suggest that rBMSCs more effectively adhere, proliferate, and differentiate on SGH surfaces. We ascribe this effect to properties of SGH films including high specific surface area, surface morphology, and the reasonable number of functional groups on the SGH film.

Stem cell growth and osteogenic differentiation might also be affected by the interaction of graphene scaffolds with osteoinductive agents in the growth medium according to a report by Lee and colleagues.[44] The present study is consistent with these results; hADSCs could attach tightly to the SGH film and appeared much flatter and more spread out than when seeded onto conventional graphene or carbon fiber films (Figure 5). After 7 days of culture, hADSCs reached confluence at the highest cell densities when seeded on SGH film. The mechanical and biological properties of the SGH film can be used to explain its biological function. With a wrinkled and rippled nanoscale structure, the SGH surface absorbs more BSA molecules than graphene or carbon fiber films after 2, 8, and 12 h of treatment. The SGH film interacted with water with a smaller contact angle that the other surfaces tested, indicating that the SGH film has a more hydrophilic surface than the other carbonaceous films (Figure 2B,C), which is a critical determinant of protein interactions with the surface. McBeath et al.[45] reported that cell shape was related to stem cell commitment to different lineages and that stem cells on graphene were spindle-shaped and possessed a higher potential for osteoblast differentiation, but this was not true of stem cells on a SiO_2 substrate. We found that the SGH film was nontoxic and biocompatible. The evidence indicates that the SGH film is more suitable for bone regeneration than graphene or carbon fiber films.

A number of studies have shown that osteoblast-specific factors might be important at several stages of bone regeneration.[46−48] In our present study, RT-PCR and immunofluorescence staining were performed to evaluate the expression of the osteogenic markers ALP, OCN, Runx2, and BMP2. In the absence of OM, cells seeded onto SGH film expressed higher levels of osteogenic specific genes such as ALP, BMP2, Runx2, and OCN than the other films tested. Cells seeded onto glass in the presence of OM had higher levels of osteogenic makers than cells on SGH film in the absence of OM. Immunofluorescence analysis also indicated that the staining for OCN, BMP2, and Runx2 was stronger for cells on SGH film than for cells on graphene, carbon fiber, or glass. Furthermore, endogenous ALP activity and cell-mediated calcium mineralization were evaluated to investigate how effectively hADSCs differentiated into osteoblasts on SGH films. Cells on SGH films had higher ALP activity than cells on other surfaces, except for the positive control, which contained cells plated on glass with OM. Mineralization, expressed as the total mineralized matrix volume, was calculated by quantifying accreted calcium for each group of cells on day 21. We found that cells on the SGH film had higher levels of accumulated calcium than cells on graphene, carbon fiber, or glass, although the mineralization of cells on the SGH film was not as high as that of cells on glass with OM (the positive control).

5. CONCLUSION

In this study, we examined the osteoinductivity of self-supporting graphene hydrogel films as an experimental platform for hADSCs. The SGH films had higher mechanical strength and higher flexibility than conventional graphene and carbon fiber films. Moreover, hADSCs exhibited better adaptation, proliferation, and differentiation on SGH surfaces than on graphene and carbon fiber films. We also found that the SGH films were nontoxic and biocompatible. The osteoinductivity of the SGH film is probably closely related to the well-spread, flat morphology of hADSCs on the SGH film, which is supported by the surface characteristics of the SGH film, forces generated at the cell/material interface, the surface hydrophilicity, and the rate of protein adsorption. Taken together, these results indicate that SGH films are a novel and self-sustaining graphene film with high potential for inducing the differentiation of ADSCs into osteoblasts.

AUTHOR INFORMATION

Corresponding Authors

*E-mail: ys-he@sjtu.edu.cn.

*E-mail: derongzou@gmail.com.

Author Contributions

¶These authors contributed equally. The manuscript was written through contributions of all authors. All authors have given approval to the final version of the manuscript.

Notes

The authors declare no competing financial interest.

ACKNOWLEDGMENTS

We are indebted to all colleagues and students who provided advice, assistance, and materials for this manuscript. This work was supported by grants from the Science and Technology Commission of Shanghai Municipality (12JC1407301, 14DZ2250800), Shanghai Natural Science Foundation (12ZR1447200), and the Natural Science Foundation of China (81470714, 31400825, 21336003).

REFERENCES

(1) Dong, H.; Dong, C.; Ren, T.; Li, Y.; Shi, D. Surface-Engineered Graphene-Based Nanomaterials for Drug Delivery. *J. Biomed. Nanotechnol.* **2014**, *10*, 2086−106.

(2) Bitounis, D.; Ali-Boucetta, H.; Hong, B. H.; Min, D. H.; Kostarelos, K. Prospects and Challenges of Graphene in Biomedical Applications. *Adv. Mater.* **2013**, *25*, 2258−68.

(3) Chen, G. Y.; Pang, D. W.; Hwang, S. M.; Tuan, H. Y.; Hu, Y. C. A Graphene-Based Platform for Induced Pluripotent Stem Cells Culture and Differentiation. *Biomaterials* **2012**, *33*, 418−27.

(4) Weaver, C. L.; Cui, X. T. Directed Neural Stem Cell Differentiation with a Functionalized Graphene Oxide Nanocomposite. *Adv. Healthcare Mater.* **2015**, *4*, 1408−16.

DOI: 10.1021/acsami.5b05802
ACS Appl. Mater. Interfaces 2015, 7, 20245−20254

(5) Lee, T. J.; Park, S.; Bhang, S. H.; Yoon, J. K.; Jo, I.; Jeong, G. J.; Hong, B. H.; Kim, B. S. Graphene Enhances the Cardiomyogenic Differentiation of Human Embryonic Stem Cells. *Biochem. Biophys. Res. Commun.* **2014**, *452*, 174−80.
(6) Hu, X.; Zhou, Q. Health and Ecosystem Risks of Graphene. *Chem. Rev.* **2013**, *113*, 3815−35.
(7) Mogharabi, M.; Abdollahi, M.; Faramarzi, M. A. Safety Concerns to Application of Graphene Compounds in Pharmacy and Medicine. *Daru, J. Pharm. Sci.* **2014**, *22*, 23.
(8) Bussy, C.; Ali-Boucetta, H.; Kostarelos, K. Safety Considerations for Graphene: Lessons Learnt from Carbon Nanotubes. *Acc. Chem. Res.* **2013**, *46*, 692−701.
(9) Lu, J. Y.; He, Y. S.; Cheng, C.; Wang, Y.; Qiu, L.; Li, D.; Zou, D. R. Self-Supporting Graphene Hydrogel Film as an Experimental Platform to Evaluate the Potential of Graphene for Bone Regeneration. *Adv. Funct. Mater.* **2013**, *23*, 3494−3502.
(10) Luo, Y.; Shen, H.; Fang, Y.; Cao, Y.; Huang, J.; Zhang, M.; Dai, J.; Shi, X.; Zhang, Z. Enhanced Proliferation and Osteogenic Differentiation of Mesenchymal Stem Cells on Graphene Oxide-Incorporated Electrospun Poly(lactic-co-glycolic acid) Nanofibrous Mats. *ACS Appl. Mater. Interfaces* **2015**, *7*, 6331−9.
(11) Crowder, S. W.; Prasai, D.; Rath, R.; Balikov, D. A.; Bae, H.; Bolotin, K. I.; Sung, H. J. Three-Dimensional Graphene Foams Promote Osteogenic Differentiation of Human Mesenchymal Stem Cells. *Nanoscale* **2013**, *5*, 4171−6.
(12) Nayak, T. R.; Andersen, H.; Makam, V. S.; Khaw, C.; Bae, S.; Xu, X.; Ee, P. L.; Ahn, J. H.; Hong, B. H.; Pastorin, G.; Özyilmaz, B. Graphene for Controlled and Accelerated Osteogenic Differentiation of Human Mesenchymal Stem Cells. *ACS Nano* **2011**, *5*, 4670−8.
(13) Yang, X.; Zhu, J.; Qiu, L.; Li, D. Bioinspired Effective Prevention of Restacking in Multilayered Graphene Films: Towards the Next Generation of High-Performance Supercapacitors. *Adv. Mater.* **2011**, *23*, 2833−8.
(14) Yang, X.; Qiu, L.; Cheng, C.; Wu, Y.; Ma, Z. F.; Li, D. Ordered Gelation of Chemically Converted Graphene for Next-Generation Electroconductive Hydrogel Films. *Angew. Chem., Int. Ed.* **2011**, *50*, 7325−8.
(15) Chen, H.; Müller, M.; Gilmore, K.; Wallace, G.; Li, D. Mechanically Strong, Electrically Conductive, and Biocompatible Graphene Paper. *Adv. Mater.* **2008**, *20*, 3557−3561.
(16) Daffonchio, D.; Thaveesri, J.; Verstraete, W. Contact Angle Measurement and Cell Hydrophobicity of Granular Sludge from Upflow Anaerobic Sludge Bed Reactors. *Appl. Environ. Microbiol.* **1995**, *61*, 3676−3680.
(17) Wang, Y.; Lu, L.; Zheng, Y.; Chen, X. Improvement in Hydrophilicity of PHBV Films by Plasma Treatment. *J. Biomed. Mater. Res., Part A* **2006**, *76A*, 589−595.
(18) Wu, C. N.; Saito, T.; Yang, Q.; Fukuzumi, H.; Isogai, A. Increase in the Water Contact Angle of Composite Film Surfaces Caused by the Assembly of Hydrophilic Nanocellulose Fibrils and Nanoclay Platelets. *ACS Appl. Mater. Interfaces* **2014**, *6*, 12707−12.
(19) Ye, X.; Zeng, Y.; Zhou, T.; Liu, F.; Liu, J.; Sha, J.; Xu, X.; Xia, L. In Situ Comparative Studies of Self-Assembly Adsorption of Bovine Serum Albumin on Nano Films by Atomic Force Microscopy. *J. Nanosci. Nanotechnol.* **2011**, *11*, 10765−9.
(20) do Serro, A. P. V. A.; Fernandes, A. C.; Saramago, B. d. J. V.; Norde, W. Bovine Serum Albumin Adsorption on Titania Surfaces and Its Relation to Wettability Aspects. *J. Biomed. Mater. Res.* **1999**, *46*, 376−81.
(21) Zeng, G.; Lai, K.; Li, J.; Zou, Y.; Huang, H.; Liang, J.; Tang, X.; Wei, J.; Zhang, P. A Rapid and Efficient Method for Primary Culture of Human Adipose-Derived Stem Cells. *Organogenesis* **2013**, *9*, 287−95.
(22) Williams, K. J.; Godke, R. A.; Bondioli, K. R. Isolation and Culture of Porcine Adipose Tissue-Derived Somatic Stem Cells. *Methods Mol. Biol.* **2011**, *702*, 77−86.
(23) Araña, M.; Mazo, M.; Aranda, P.; Pelacho, B.; Prosper, F. Adipose Tissue-Derived Mesenchymal Stem Cells: Isolation, Expansion, and Characterization. *Methods Mol. Biol.* **2013**, *1036*, 47−61.
(24) Lin, K.; Matsubara, Y.; Masuda, Y.; Togashi, K.; Ohno, T.; Tamura, T.; Toyoshima, Y.; Sugimachi, K.; Toyoda, M.; Marc, H.; Douglas, A. Characterization of Adipose Tissue-Derived Cells Isolated with the Celution System. *Cytotherapy* **2008**, *10*, 417−26.
(25) Martin-Piedra, M. A.; Garzon, I.; Oliveira, A. C.; Alfonso-Rodriguez, C. A.; Carriel, V.; Scionti, G.; Alaminos, M. Cell Viability and Proliferation Capability of Long-Term Human Dental Pulp Stem Cell Cultures. *Cytotherapy* **2014**, *16*, 266−77.
(26) Grausova, L.; Kromka, A.; Burdikova, Z.; Eckhardt, A.; Rezek, B.; Vacik, J.; Haenen, K.; Lisa, V.; Bacakova, L. Enhanced Growth and Osteogenic Differentiation of Human Osteoblast-Like Cells on Boron-Doped Nanocrystalline Diamond Thin Films. *PLoS One* **2011**, *6*, e20943.
(27) Yourek, G.; McCormick, S. M.; Mao, J. J.; Reilly, G. C. Shear Stress Induces Osteogenic Differentiation of Human Mesenchymal Stem Cells. *Regener. Med.* **2010**, *5*, 713−24.
(28) Thibault, R. A.; Scott Baggett, L.; Mikos, A. G.; Kasper, F. K. Osteogenic Differentiation of Mesenchymal Stem Cells on Pregenerated Extracellular Matrix Scaffolds in the Absence of Osteogenic Cell Culture Supplements. *Tissue Eng., Part A* **2010**, *16*, 431−40.
(29) Jaiswal, N.; Haynesworth, S. E.; Caplan, A. I.; Bruder, S. P. Osteogenic Differentiation of Purified, Culture-Expanded Human Mesenchymal Stem Cells *in Vitro*. *J. Cell. Biochem.* **1997**, *64*, 295−312.
(30) Hale, L. V.; Ma, Y. F.; Santerre, R. F. Semi-Quantitative Fluorescence Analysis of Calcein Binding as a Measurement of *in Vitro* Mineralization. *Calcif. Tissue Int.* **2000**, *67*, 80−4.
(31) Ramírez-Zacarías, J. L.; Castro-Muñozledo, F.; Kuri-Harcuch, W. Quantitation of Adipose Conversion and Triglycerides by Staining Intracytoplasmic Lipids with Oil Red O. *Histochemistry* **1992**, *97*, 493−497.
(32) Kapur, S. K.; Dos-Anjos Vilaboa, S.; Llull, R.; Katz, A. J. Adipose Tissue and Stem/Progenitor Cells: Discovery and Development. *Clin Plast Surg.* **2015**, *42*, 155−67.
(33) Wang, W. W.; Li, Z. Z.; Wang, W.; Jiang, Y.; Cheng, J.; Lu, S.; Zhang, J. Y. Enhanced Renoprotective Effect of HIF-1α Modified Human Adipose-Derived Stem Cells on Cisplatin-Induced Acute Kidney Injury. *Sci. Rep.* **2015**, *5*, 10851.
(34) Lin, G.; Wang, G.; Liu, G.; Yang, L. J.; Chang, L. J.; Lue, T. F.; Lin, C. S. Treatment of Type 1 Diabetes with Adipose Tissue-Derived Stem Cells Expressing Pancreatic Duodenal Homeobox 1. *Stem Cells Dev.* **2009**, *18*, 1399−406.
(35) Kajiyama, H.; Hamazaki, T. S.; Tokuhara, M.; Masui, S.; Okabayashi, K.; Ohnuma, K.; Yabe, S.; Yasuda, K.; Ishiura, S.; Okochi, H.; Asashima, M. Pdx1-Transfected Adipose Tissue-Derived Stem Cells Differentiate into Insulin-Producing Cells *in Vivo* and Reduce Hyperglycemia in Diabetic Mice. *Int. J. Dev. Biol.* **2010**, *54*, 699−705.
(36) Nam, J. S.; Kang, H. M.; Kim, J.; Park, S.; Kim, H.; Ahn, C. W.; Park, J. O.; Kim, K. R. Transplantation of Insulin-Secreting Cells Differentiated from Human Adipose Tissue-Derived Stem Cells into Type 2 Diabetes Mice. *Biochem. Biophys. Res. Commun.* **2014**, *443*, 775−81.
(37) Howard, D.; Buttery, L. D.; Shakesheff, K. M.; Roberts, S. J. Tissue Engineering: Strategies, Stem Cells and Scaffolds. *J. Anat.* **2008**, *213*, 66−72.
(38) Park, H. J.; Yu, S. J.; Yang, K.; Jin, Y.; Cho, A. N.; Kim, J.; Lee, B.; Yang, H. S.; Im, S. G.; Cho, S. W. Paper-Based Bioactive Scaffolds for Stem Cell-Mediated Bone Tissue Engineering. *Biomaterials* **2014**, *35*, 9811−23.
(39) Boccaccini, A. R.; Kneser, U.; Arkudas, A. Scaffolds for Vascularized Bone Regeneration: Advances and Challenges. *Expert Rev. Med. Devices* **2012**, *9*, 457−60.
(40) Li, X.; Wang, L.; Fan, Y.; Feng, Q.; Cui, F. Z.; Watari, F. Nanostructured Scaffolds for Bone Tissue Engineering. *J. Biomed. Mater. Res., Part A* **2013**, *101A*, 2424−2435.
(41) Nair, M.; Nancy, D.; Krishnan, A. G.; Anjusree, G. S.; Vadukumpully, S.; Nair, S. V. Graphene Oxide Nanoflakes Incorporated Gelatin-Hydroxyapatite Scaffolds Enhance Osteogenic Differentiation of Human Mesenchymal Stem Cells. *Nanotechnology* **2015**, *26*, 161001.

DOI: 10.1021/acsami.5b05802
ACS Appl. Mater. Interfaces 2015, 7, 20245−20254

(42) Jung, H. S.; Lee, T.; Kwon, I. K.; Kim, H. S.; Hahn, S. K.; Lee, C. S. Surface Modification of Multipass Caliber-Rolled Ti Alloy with Dexamethasone-Loaded Graphene for Dental Applications. *ACS Appl. Mater. Interfaces* **2015**, *7*, 9598−607.
(43) Wall, I.; Donos, N.; Carlqvist, K.; Jones, F.; Brett, P. Modified Titanium Surfaces Promote Accelerated Osteogenic Differentiation of Mesenchymal Stromal Cells. *in Vitro. Bone.* **2009**, *45*, 17−26.
(44) Lee, W. C.; Lim, C. H.; Shi, H.; Tang, L. A.; Wang, Y.; Lim, C. T.; Loh, K. P. Origin of Enhanced Stem Cell Growth and Differentiation on Graphene and Graphene Oxide. *ACS Nano* **2011**, *5*, 7334−41.
(45) McBeath, R.; Pirone, D. M.; Nelson, C. M.; Bhadriraju, K.; Chen, C. S. Cell shape, Cytoskeletal Tension, and RhoA Regulate Stem Cell Lineage Commitment. *Dev. Cell* **2004**, *6*, 483−95.
(46) Cowan, C. M.; Jiang, X.; Hsu, T.; Soo, C.; Zhang, B.; Wang, J. Z.; Kuroda, S.; Wu, B.; Zhang, Z.; Zhang, X.; Ting, K. Synergistic Effects of Nell-1 and BMP-2 on the Osteogenic Differentiation of Myoblasts. *J. Bone Miner. Res.* **2007**, *22*, 918−30.
(47) Luu, H. H.; Song, W. X.; Luo, X.; Manning, D.; Luo, J.; Deng, Z. L.; Sharff, K. A.; Montag, A. G.; Haydon, R. C.; He, T. C. Distinct Roles of Bone Morphogenetic Proteins in Osteogenic Differentiation of Mesenchymal Stem Cells. *J. Orthop. Res.* **2007**, *25*, 665−77.
(48) Granchi, D.; Ochoa, G.; Leonardi, E.; Devescovi, V.; Baglìo, S. R.; Osaba, L.; Baldini, N.; Ciapetti, G. Gene Expression Patterns Related to Osteogenic Differentiation of Bone Marrow-Derived Mesenchymal Stem Cells during *ex Vivo* Expansion. *Tissue Eng., Part C* **2010**, *16*, 511−24.

DOI: 10.1021/acsami.5b05802
ACS Appl. Mater. Interfaces 2015, 7, 20245−20254